JOURNAL OF ENVIRONMENTAL SCIENCES 138 (2024) 406–417

Available online at www.sciencedirect.com

ScienceDirect

www.elsevier.com/locate/jes

JES JOURNAL OF ENVIRONMENTAL SCIENCES

www.jesc.acn

Research Article

Elaborations of the influencing factors on the formation of secondary inorganic aerosols in a heavily polluted urban area of China

Shuang Wang[1,2], *Qiyuan Wang*[2,3,4,*], *Ting Zhang*[2,3], *Suixin Liu*[2,3], *Steven Sai Hang Ho*[5,6], *Jie Tian*[2,3], *Hui Su*[7], *Yong Zhang*[2], *Luyao Wang*[7], *Tingting Wu*[7], *Junji Cao*[8,*]

[1] *School of Human Settlements and Civil Engineering, Xi'an Jiaotong University, Xi'an 710049, China*
[2] *Key Laboratory of Aerosol Chemistry and Physics, State Key Laboratory of Loess and Quaternary Geology, Institute of Earth Environment, Chinese Academy of Sciences, Xi'an 710061, China*
[3] *CAS Center for Excellence in Quaternary Science and Global Change, Xi'an 710061, China*
[4] *National Observation and Research Station of Regional Ecological Environment Change and Comprehensive Management in the Guanzhong Plain, Xi'an 710061, China*
[5] *Division of Atmospheric Sciences, Desert Research Institute, Reno, Nevada, 89512, United States*
[6] *Hong Kong Premium Services and Research Laboratory, Kowloon, Hong Kong SAR, China*
[7] *Xi'an Institute for Innovative Earth Environment Research, Xi'an 710061, China*
[8] *Institute of Atmospheric Physics, Chinese Academy of Sciences, Beijing 100029, China*

ARTICLE INFO

Article history:
Received 20 February 2022
Revised 14 March 2023
Accepted 14 March 2023
Available online 25 March 2023

Keywords:
Haze episodes
Secondary inorganic aerosol
Secondary conversion ratio
Meteorological factors

ABSTRACT

In this study, online water-soluble inorganic ions were detected to deduce the formation mechanism of secondary inorganic aerosol in Xianyang, China during wintertime. The dominant inorganic ions of sulfate (SO_4^{2-}), nitrate (NO_3^-), and ammonium (NH_4^+) (the sum of those is abbreviated as SNA) accounted for 17%, 21%, and 12% of $PM_{2.5}$ mass, respectively. While the air quality deteriorated from excellent to poor grades, the precursor gas sulfur dioxide (SO_2) of SO_4^{2-} increased and then decreased with a fluctuation, while nitrogen dioxide (NO_2) and ammonia (NH_3), precursors of NO_3^- and NH_4^+, and SNA show increasing trends. Meteorological factors including boundary layer height (BLH), temperature, and wind speed also show decline trends, except relative humidity (RH). Meanwhile, the secondary conversion ratio shows a remarkable increasing trend, indicating that there was a strong secondary transformation. From the perspective of chemical mechanisms, RH is positively correlated with sulfur oxidation ratios (SOR), nitrogen oxidation ratios (NOR), and ammonia conversion ratios, representing that the increase of humidity could promote the generation of SNA. Notably, SOR and NOR were also positively related to the ammonia. On the one hand, the low wind speed and BLH led to the accumulation of pollutants. On the other hand, the increases of RH and ammonia promoted more formations of SNA and $PM_{2.5}$. The results

* Corresponding authors.
E-mails: wangqy@ieecas.cn (Q. Wang), jjcao@mail.iap.ac.cn (J. Cao).

https://doi.org/10.1016/j.jes.2023.03.022

advance our identification of the contributors to the haze episodes and assist to establish more efficient emission controls in Xianyang, in addition to other cities with similar emission and geographical characteristics.

Introduction

In recent years, haze has become one of the prominent atmospheric pollution issues in many Chinese cities or regions, especially $PM_{2.5}$ (i.e., particulate matter with an aerodynamic diameter less than 2.5 μm) is considered a "culprit". High concentrations levels of $PM_{2.5}$ have critical influences on ecology (Cheng et al., 2021), atmospheric visibility (Liu et al., 2019a; Wang et al., 2013), and public health (Bei et al., 2021; Han et al., 2021; Sinha and Kumar, 2019).

Many research results showed that secondary inorganic aerosol (e.g., sulfate (SO_4^{2-}), nitrate (NO_3^-), and ammonium (NH_4^+)) accounted for a high proportion in $PM_{2.5}$ mass, and even reached up to 60% during haze episodes (Liu et al., 2019b; Tian et al., 2017). In some areas of China, the ambient concentration of SO_4^{2-} declined 31% in comparison to that 10 years ago, but NO_3^- has doubled up, attributed to a continual and substantial increase of fine particle emissions from automobiles (Tian et al., 2017). Sulfur dioxide (SO_2), nitrogen dioxide (NO_2), and ammonia (NH_3) not only are the precursors of the SNA, respectively, but could be interacted with each other. NH_3 is the main alkaline gas in the atmosphere and plays an important role in the formation of haze. It can promote the heterogeneous reactions of SO_2 and NO_2, elevate the production of nitrous acid (HONO), and then facilitate the oxidation capacity (Ox) (Jain et al., 2022; Pancholi et al., 2018) of the atmosphere (Ge et al., 2019b; Kuang et al., 2020; Wu et al., 2020). It is a critical participant in secondary pollutant formation. NH_4^+ is the most important cation in the chemical composition of $PM_{2.5}$ which promotes the growth of $PM_{2.5}$ by neutralizing the anions such as SO_4^{2-} and NO_3^-, but it preferentially combined with SO_4^{2-} in high RH, thus the formation of NO_3^- was also affected by the mass concentration of both NH_3 and SO_2 (Feng et al., 2018; Wang et al., 2016a; Xia et al., 2016) . During the heavy pollution, the portion of NH_x (accounting for both gaseous NH_3 and the particulate NH_4^+) mostly exceeded that of the SO_4^{2-}-NO_3^--NH_4^+ equilibrium system. Excessive NH_x could cause aerosols to be moderately acidic and consequently promote the formation of particulate-phase NO_3^-. Furthermore, especially at nighttime, excessive NH_x can also advance the generation of ammonium nitrate (NH_4NO_3) which facilitates hygroscopic growth when relative humidity (RH) is below 50% (Ge et al., 2019a). The wet aerosol particles become a good mediator for rapid multiphase reactions. The incessant increase of RH can accelerate the production ratio of SO_4^{2-} and hydrolysis of NO_2 to HONO, further releasing large numbers of OH Free radicals (•OH), which initiate the atmospheric photochemical reactions and formations of secondary aerosols (Ge et al., 2019a; Wang et al., 2016a; Xu et al., 2019). Therefore, the chain reactions cause the explosive growth of NO_3^- and haze. Water content also plays an important role in the formation of secondary aerosols. Some researchers claimed that RH has a great influence on the degree of oxidations of sulfur and nitrogen-containing compounds, advocating the formation of secondary inorganic aerosols (Tian et al., 2017; Zhan et al., 2021). Others reported that the influence of liquid phase reaction on the secondary aerosols was complex under a variety of RHs in different pollution events (Tian et al., 2021; Zhang et al., 2021). There was a strong linear correlation between aerosol liquid water content (ALWC) and sulfur oxidation ratios, nitrogen oxidation ratios (denoted as SOR and NOR, respectively), while a logarithmic relationship between ALWC and ammonia conversion ratios (NHR) during the heavy $PM_{2.5}$ pollutions (Zhang et al., 2021). Their results conclude that the influence of water content on SNA is worth further exploration.

The Guanzhong Basin is one of the regions that show the worst air pollution in China (Bei et al., 2021). Of the most polluted city in Guanzhong Plain, Xianyang had an average annual $PM_{2.5}$ concentration of 74 μg/m^3 in 2016, twice exceeding the China National Ambient Air Quality Grade II Standard (35 μg/m^3, GB 3095-2012). And there are more than 40 heavily polluted days in a year. The air quality has been significantly improved with the implementation of multiple emission control measure projects for heavy air pollution during 2018-2020. The improvement could be acknowledged by that it ranks third in terms of air quality improvement amplitude among 168 major Chinese cities in 2019 and ranks first in terms of air quality improvement rate among the cities of Guanzhong Basin in 2020. The annual average mass concentration of $PM_{2.5}$ declined to 54 μg/m^3 in 2020 but still exceeded the Standard. Therefore, atmospheric pollution is still not optimistically solved in Xianyang. In addition, due to the increases in demands of local fuel combustions and adverse meteorological conditions, haze episodes still frequently occur in Xianyang during wintertime. However, limited studies have been conducted to interpret the causes of the pollution and determine the formation mechanism of haze pollution in this city (Bei et al., 2016; Li et al., 2022; Zhao et al., 2020).

To better explore the characteristics of chemical composition, the formation mechanism of SNA, and consequent atmospheric reactions in the formation of haze pollution in Xianyang, an online In-situ Gas, and Aerosol Composition (IGAC) analyzer was used to determine inorganic water-soluble ions and gases in this study. With the atmospheric parameters, the secondary conversion ratios at different levels of heavy haze events were determined. In addition, the relationships between ammonia, RH, and the secondary conversion ratios were elaborated. The key objective is to acquire a comprehensive and profound understanding of the formation mechanism of hazes and the roles of SNA in the Guanzhong Plain during haze episodes. This could provide a more precise scientific basis for the prevention and control of local air pollution.

1. Material and methods

1.1. Sampling site

Xianyang City (107°38′E-109°10′E, 34°11′N-35°32′N) is located in the hinterland of the Guanzhong Plain, northwest China. To the south is the Qinling Mountains, and to the north is the hilly-gully region of the Loess Plateau, which is vulnerable to exposures of loess. The terrain of Xianyang is high in the north and low in the south. The urban area is close to the Valley of Weihe River, with a low elevation. The prevailing wind is from the northeast, and the airflow is often blocked by the Qinling Mountains, resulting in poor air dispersion. According to the SHAANXI STATISTICAL YEARBOOK of 2020 and XIANYANG STATISTICAL YEARBOOK of 2020, the area of Xianyang is ca. 9544 km^2 and had a population size of ca. 4350,000 and a motor vehicles number of ~500,000. Therefore, the total amounts of anthropogenic emissions such as $PM_{2.5}$ are relatively high, resulting in frequent occurrences of heavy air pollution.

The sampling site (34°19′N, 108°39′E) is in downtown Xianyang which is close to many large construction sites. It is well represented a place, which was undergone modernization in this developing city (Appendix A Fig. S1). The IGAC instrument was situated on the rooftop of a building of the Xinyuan Youyicheng Community, which is ~106 m above ground level and beyond the Valley of Weihe River. The mid-altitude sampling site can effectively reduce the impact of the local ground-levels pollution and air dispersion from buildings. Therefore, this could better monitor the spatial scale pollution conditions of Xianyang.

1.2. Sampling and instrument descriptions

The observation period is from December 30th, 2018, to January 19th, 2019, when two haze episodes occurred between the period. The concentrations of water-soluble inorganic ions (denoted as WSII, including Cl^-, NO_3^-, NO_2^-, NH_4^+, SO_4^{2-}, F^-, Na^+, K^+, Mg^{2+}, Ca^{2+}, and Br^-) in $PM_{2.5}$ and gases (i.e., HCl, NH_3, HNO_3, and organic acids) were simultaneously measured using an IGAC (Model S-611, Fortelice International Co., Taiwan, China) with a time resolution of 1 hr. The operation principle of the IGAC has been shown in detail elsewhere (Zhang et al., 2021). In brief, the IGAC mainly consists of an annular denuder (WAD), a scrub and impact aerosol collector (SCI), and ion chromatography (IC). The operation flow rate was 16.67 L/min. The gases and aerosols were separated by the WAD and SCI, respectively. The air drawn by the WAD was wetted with a dilute 5 mmol hydrogen peroxide (H_2O_2) solution. The SCI was located under the WAD, and its effects mainly included wet scrubbing, particle condensation growth, and impaction to capture particles. The gas and aerosol solutions from the WAD and SCI were subsequently extracted and simultaneously quantified for both ions by the IC with a time interval of 1 hr. For the equipped IC, two AS9-HC and CS12A analytical columns were utilized to separate anions and cations, respectively. The collection efficiency of IGAC for the target species is generally higher than 80% (Chang et al., 2007). The method detection limit (MDL) for $PM_{2.5}$ water-soluble ions was below 0.12 μg/m^3 (main ions' MDLs were shown in Table 1), and background levels were mostly below the LOD (< 0.11 μg/m^3), except SO_4^{2-} (1.10 μg/m^3) (Pang et al., 2021; Young et al., 2016).

Table 1 – The method detection limit (MDL) for main water-soluble inorganic ions by IGAC (unit: μg/m^3).

Ions	NO_3^-	NH_4^+	Cl^-	K^+	SO_4^{2-}	Na^+	Mg^{2+}	Ca^{2+}
MDL	0.05	0.05	0.05	0.05	0.04	0.04	0.04	0.04

1.3. Collections of $PM_{2.5}$, gases, and meteorological parameters

Air quality data of hourly $PM_{2.5}$, SO_2, and NO_2 mass concentrations, as well as meteorological data including RH, temperature (T), air pressure (P), wind speed (WS), and wind direction (WD), were collected from the Air Quality Network Monitoring and Management platform in the Shaanxi Province (http://221.11.17.250:9000). The station was ~1.6 km southeast of our sampling site. Boundary layer height in this study was achieved from the ERA5 hourly data on single levels in the website of https://cds.climate.copernicus.eu/cdsapp#!/home.

2. Results and discussion

2.1. Characteristics of pollutants in Xianyang

2.1.1. $PM_{2.5}$ concentration

The time series of hourly concentrations of $PM_{2.5}$ in Xianyang during the entire observation period is shown in Appendix A Fig. S2. The average mass concentration of $PM_{2.5}$ is 182.3 ± 97.4 μg/m^3. The city experienced two haze episodes (i.e., the hourly concentration of $PM_{2.5}$ exceeded 150 μg/m^3) within the observation period when the atmospheric pollution covered a large scope and prolonged.

The first haze episode occurred from 21:00 on December 31st, 2018 to 11:00 on January 7th, 2019. During ~157 hr, the $PM_{2.5}$ concentrations exceed 150 μg/m^3, with average and peak concentrations of 268.0 and 427.0 μg/m^3, respectively. The second haze episode happened from 11:00 on January 10th, 2019 to 03:00 on January 15th, 2019. There are 96 hr that exceeded the $PM_{2.5}$ guideline, while the hourly average and peak concentration levels are 240.8 and 397.0 μg/m^3, respectively.

2.1.2. Ionic concentrations

Table 2 lists the average mass concentrations of the target WSII in $PM_{2.5}$ during the observation period. The average hourly mass concentration of total WSIIs is 95.4 ± 54.8 μg/m^3, accounting for 52% of $PM_{2.5}$. The mass concentrations of individual WSII show a descending order of $NO_3^- > NH_4^+ > SO_4^{2-} > Cl^- > K^+ > Na^+ = Mg^{2+} > Ca^{2+}$ > others. The most abundant WSII is NO_3^-, with an average concentration of 36.6 ± 23.3 μg/m^3 and accounts for 19% to the $PM_{2.5}$, followed by NH_4^+ (30.2 ± 17.3 μg/m^3, 17%), and SO_4^{2-} (21.4 ± 12.7 μg/m^3, 13%). The sum of SNA has a contribution of ~49% of $PM_{2.5}$ attributed to the strong secondary conversion from their precursor gases

Table 2 – Average mass concentration of water-soluble inorganic ions in $PM_{2.5}$ during the observation period (unit: μg/m³).

Time event	Ions							
	NO_3^-	NH_4^+	SO_4^{2-}	Cl^-	K^+	Na^+	Mg^{2+}	Ca^{2+}
First haze episode	55.9±16.4	43.6±11.8	32.1±9.6	6.0±1.3	3.2±1.0	0.3±0.3	0.2±0.1	0.1±0.2
Second haze episode	52.8±15.7	44.3±10.8	30.2±8.9	5.3±1.7	3.1±1.1	0.2±0.2	0.2±0.1	0.0±0.0
Observation period	36.6±23.3	30.2±17.3	21.4±12.7	4.7±1.9	2.2±1.3	0.2±0.2	0.2±0.1	0.0±0.1

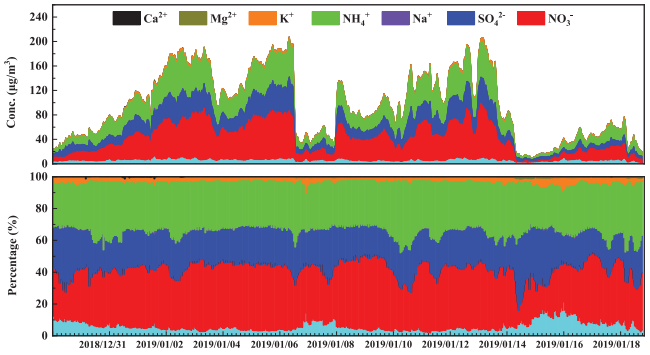

Fig. 1 – Hourly concentrations and proportions of inorganic water-soluble ions in $PM_{2.5}$ during the observation period.

including SO_2, NOx, and NH_3. In addition, the accumulation of NO_3^- is significantly greater than that of SO_4^{2-} during the observation period.

Fig. 1 illustrates the mass concentration trends of NO_3^-, SO_4^{2-}, and NH_4^+ during the observation period which is perceptibly consistent with $PM_{2.5}$, especially from 00:00 on December 30th to 02:00 on January 3rd. Across this period, the $PM_{2.5}$ concentration rapidly rises from 47 to 380 μg/m³, showing an increase of 7.1 fold. The mass concentration of SNA increases simultaneously, in which SO_4^{2-} increases from 6.2 to 43.4 μg/m³ (6.0 fold), NO_3^- increases from 7.9 to 64.3 μg/m³ (7.2 fold), and NH_4^+ increases from 7.2 to 56.1 μg/m³ (6.7 fold).

The average mass concentrations of Cl^- and K^+ are 4.7 ± 1.9 and 2.2 ± 1.3 μg/m³, with mass proportions of 3% and 1%, respectively, in the $PM_{2.5}$ during the entire observation period. Their contributions are closely related to the coal combustion and biomass burning applied for heating in Xianyang and surrounding areas in wintertime (Lobert et al., 1999; Shen et al., 2008). The mass concentrations of other metal ions are relatively low. The average concentrations of Na^+, Mg^{2+}, and Ca^{2+} are 0.2 ± 0.2, 0.2 ± 0.1, and 0.0 ± 0.1 μg/m³, and their mass proportions in $PM_{2.5}$ are all below 0.2%. As shown in Table 2, although the percentage of metal ions is relatively low, they could compete with NH_x to participate in neutralization with sulfate and nitrate or reduce aerosol acidity and drive HNO_3 into the particle phase, finally promoting the formation of nitrate (Allen et al., 2015; Huang et al., 2020). Therefore, it might have a significant effect on the reaction of secondary aerosols. A more in-depth investigation is required to explore the correlation between the changes of metal ions and inorganic ions in future studies.

2.1.3. Characteristics of SNA, gases, and meteorological parameters in different pollution levels

To better determine the pollutants formations and interactions, the pollution development was divided into six levels according to the mass concentration of $PM_{2.5}$ from low to high: (1) Excellent: $PM_{2.5} \leq 35$ μg/m³, (2) Good: 35 μg/m³ < $PM_{2.5} \leq$ 75 μg/m³, (3) Light pollution: 75 μg/m³ < $PM_{2.5} \leq 115$ μg/m³, (4) Medium pollution: 115 μg/m³ < $PM_{2.5} \leq 150$ μg/m³, (5) Heavy pollution: 150 μg/m³ < $PM_{2.5} \leq 250$ μg/m³, and (6) Severe pollution: $PM_{2.5} > 250$ μg/m³.

As shown in Fig. 2, along with the air qualities from the Excellent to Severe levels, the gas precursors NO_2 and NH_3 show a constantly increasing trend, from 10.5 ± 3.3 to 26.0 ± 11.2 μg/m³ (a 148% increase) and 34.5 ± 8.7 to 77.4 ± 16.3 μg/m³ (a 124% increase), respectively. For SO_2, it increases from Excellent to Good (12.1 ± 2.9 to 21.0 ± 3.6 μg/m³) but shows a fluctuating downward trend from Good to Severe pollution levels. The average concentration of SO_2 during Severe pollution (12.0 ± 3.6 μg/m³) is even lower than that during the Excellent level.

The SNA showed an exponentially upward trend along with the aggravation of pollution levels. The average concentration of NO_3^- rises dramatically from 3.8 ± 2.2 to 66.7 ± 10.5 μg/m³ along with the Excellent to Severe pollution levels. The growth rate is as high as 1,635%. For NH_4^+, it had a growth rate of 931% from the Excellent (5.0 ± 2.4 μg/m³) to Severe pollution (51.8 ± 7.3 μg/m³). A minimal increase of 624% is shown for SO_4^{2-}, which rises from 5.3 ± 1.3 to 38.1 ± 5.9 μg/m³ along with the same pollution levels.

In terms of meteorological parameters, T shows a fluctuant downward trend from -0.2 ± 2.5 to 2.2 ± 3.3°C, while P ranges from 979.8 ± 3.7 to 984.4 ± 4.3 hPa. Both T and P have no obvious and consistent changes. Meanwhile, WS presents a continual downward trend, with the largest decline of 50%, occurring from the levels of Excellent (2.7 ± 1.0 m/sec) to Light pollution (1.4 ± 0.6 m/sec). From Light to Severe pollution, WS is close to the calm wind (1 m/sec) and shows a slight downward trend continuously. Notably, the WS reduces to 1.1 ± 0.6 m/sec during Severe pollution, representing extremely poor air dispersion horizontally. The BLH exhibits a fluctuating downward trend and the largest decline of 62.8% occurred from the Excellent to Medium pollution, from 579.7 ± 518.1 m to 215.7 ± 262.8 m. From the Medium to Severe pollutions, the average values of BLH are < 250 m and even a minimum of 182.9 m, inconducive to vertical air dispersion. However, RH shows a reverse trend with other meteorological factors, showing upwards of 28.5% ± 4.9% to 74.7% ± 9.6% from the Excellent to Severe pollution levels. Ox, the sum of O_3 and NO_2 concentrations (Alghamdi et al., 2014; Clapp and Jenkin, 2001; Jenkin, 2014), is

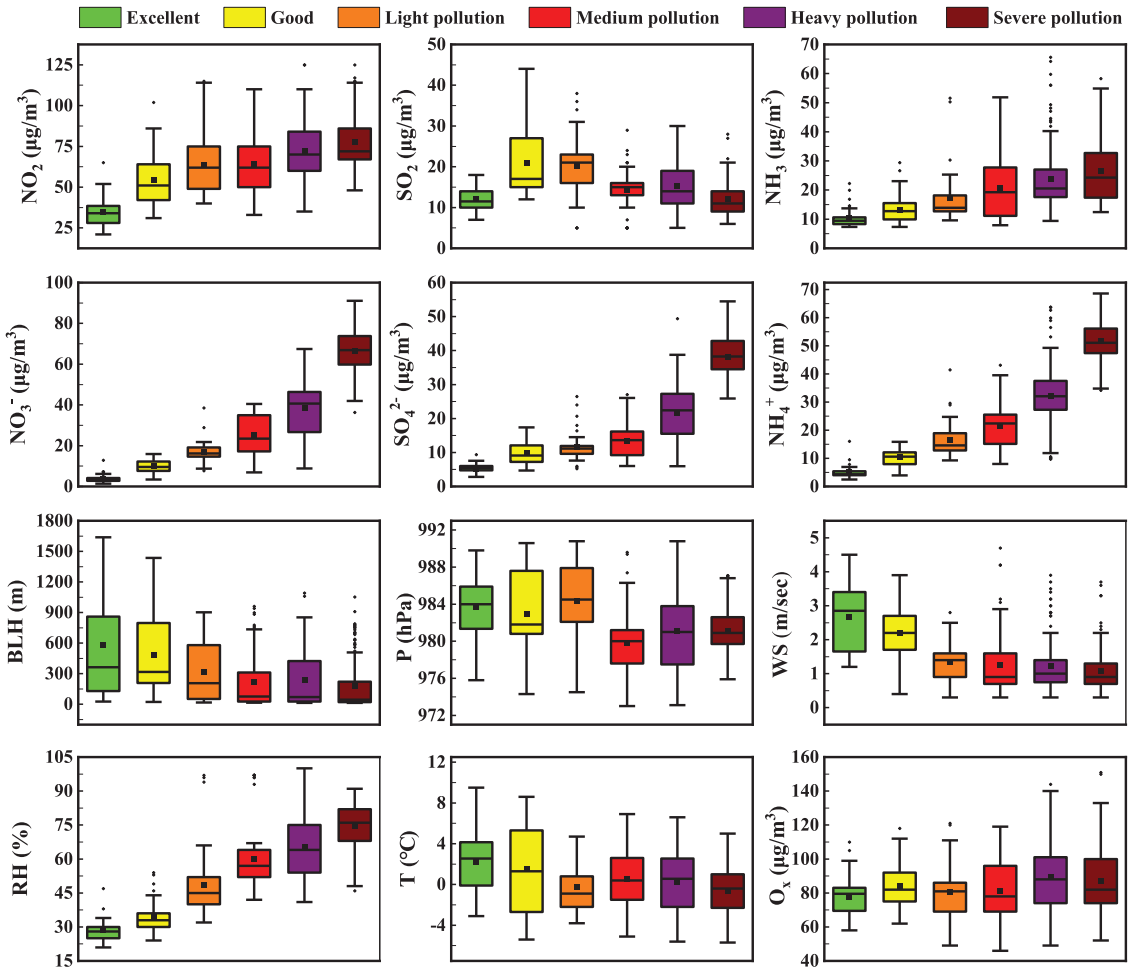

Fig. 2 – Box plots of gas precursors (NO_2, SO_2, and NH_3), secondary conversion ratio (NOR, SOR, and NHR), Ox, meteorological parameters (temperature, relative humidity, air pressure, wind speed, and boundary layer height), and SNA (NO_3^-, SO_4^{2-}, and NH_4^+) at different pollution levels.

a proxy for atmospheric oxidation capacity in the troposphere, which also presented a fluctuating upward trend with relatively small changes. The minimum Ox is 77.9 ± 11.8 μg/m^3 during the Excellent level, while the maximum 89.4 ± 20.7 μg/m^3 is seen during the Severe pollution.

The formation of haze episodes could be closely related to the reduction of BLH in vertical and WS in horizontal directions, causing the difficult spread of air pollutants. In addition, SNA is simply generated due to the liquid-phase chemical reaction in a high RH environment. Both these factors facilitate the growth of $PM_{2.5}$.

The molar ratio of NO_3^- to SO_4^{2-} can be used to indicate the relative importance of stationary and mobile pollution sources in the atmosphere (Cao et al., 2012; Wang et al., 2016b). If the ratio of NO_3^-/SO_4^{2-} is greater than 1.0, it represents that the pollution mainly originated from mobile sources; Otherwise, the pollution is mainly from stationary sources (Zhan et al., 2021).

During the entire observation period, 94% of the hourly ratio of NO_3^-/SO_4^{2-} is greater than 1.0, with an average of 2.6 ± 0.1, suggesting that the contribution of mobile sources is much greater than that of stationary sources in Xianyang. As illustrated in Fig. 3, the ratios show an increase of 150% from 1.2 ± 0.5 during the Excellent to 3.0 ± 0.7 during Medium pollution. The overwhelming ratio of NO_3^-/SO_4^{2-} could be attributed to the stronger emission of NO_x than SO_2 in the study area as well as the fast conversion under the high RH due to

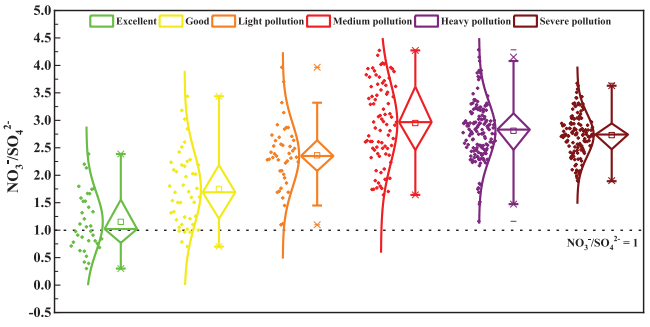

Fig. 3 – Box plots of the ratio of NO_3^-/SO_4^{2-} at different pollution levels.

the liquid-phase reaction. Detailed formation mechanism can be found in Section 2.2. Meanwhile, with the increase of RH, the growth rate of NO_3^- is higher than that of SO_4^{2-}. However, during the Medium pollution to Severe pollution, the NO_3^-/SO_4^{2-} ratios exhibit a slight downward trend, potentially limited by the factor of humidity as above mentioned. It should be noted that more than 32% of the days with RH > 80% during the Severe pollution period, in comparison to only 16% during the Heavy pollution. Those possibly led to a decrease in NO_3^- formation compared to SO_4^{2-}, resulting in a decrease of the NO_3^-/SO_4^{2-} ratio.

2.1.4. *Impacts of wind speeds and wind directions*

The general WS is lower than 1.0 m/sec in Xianyang in wintertime, which is ~50% higher than that during the observation period. To explore the relationships between the concentrations of $PM_{2.5}$, NO_3^- SO_4^{2-}, and NH_4^+ and the WS in the horizontal direction further, bivariate polar plots were utilized and presented in Appendix A Fig. S3. As shown, the high levels of pollutants mainly concentrate at low WS (<1.5 m/sec), supported the accumulation of pollutants from local emissions under a poor air dispersion environment. With the higher WS, the concentrations of the pollutants are significantly higher in the northeast than in the southwest. This could be ascribed to less local emission and better air dispersion in the southwest. Besides, the WD also governs the dilutions of air pollutants. While the airflow prevailed from the northeast, more pollutants would be transported to the polluted areas and resulting in further poor air quality in urban Xianyang.

2.2. *Formation mechanism of SNA*

Fig. 4 illustrates the molar concentrations of NH_4^+ versus SO_4^{2-} and NO_3^-, respectively, during the observation period. The NH_4^+ versus SO_4^{2-} presents a notable linear correlation ($R^2 = 0.923$), with a slope $[SO_4^{2-}] = 0.1323[NH_4^+] + 0.0014$. A significant correlation ($R^2 = 0.858$) is also observed between the molar concentrations of NH_4^+ versus NO_3^-, with a slope of $[NO_3^-] = 0.3622\ [NH_4^+]$ - 0.0169. The strong correlations support that these three ions mainly exist in form of NH_4NO_3 and $(NH_4)_2SO_4$. The average concentration of NH_3 is 21.5 ± 10.8 μg/m^3, ranging from 7.3 to 65.6 μg/m^3. Free-NH_3 which represents the degree of ammonia-rich could be determined by the following equation (Huang et al., 2021).

$$[\text{Free} - NH_3] = [NH_3] + [NH_4^+] - 2[SO_4^{2-}] \quad (1)$$

where [Free-NH_3] (μmol/m^3) is the molar concentration of Free-NH_3, [NH_3] (μmol/m^3) is ammonia gas molar concentration, and [NH_4^+] (μmol/m^3) and [SO_4^{2-}] (μmol/m^3) are the molar concentration of particulate ammonium and sulfate, respectively. The average concentration of Free-NH_3 is 2.5 ± 1.2 μmol/m^3, with a maximum of 6.6 μmol/m^3. The values further suggest that Free-NH_3 is rich during the entire observation period.

China is a key NH_3 emission country on a global scale. The North China Plain and Xi'an city, the capital city of Shaanxi province, show ammonia enrichment in the atmosphere, identical to the situation of Xianyang city (Liu et al., 2017; Wen et al., 2021; Zhang et al., 2017, 2021). The ammonia-rich environment is common which could promote the heterogeneous reaction of SO_2 with NO_2, and lead to the formation of atmospheric HONO (Ge et al., 2019b). Furthermore, the degree of ammonia-rich plays an important role in gas-particle distribution that influences the second formation of weakly acidic fine particles during haze episodes (Liu et al., 2017). There is a report that if the NH_3 emissions are reduced by 20%, the $PM_{2.5}$ mass concentration could be reduced by 5%-11% (Ge et al., 2019a). Therefore, the reduction of ammonia emissions is a measure to prevent haze episodes (Liu et al., 2019b).

In general, SO_2 can be converted to particulate SO_4^{2-} through liquid-phase reaction or gas-phase oxidation by OH radicals (•OH). The formation of NO_3^- is from liquid phase oxidation reactions or the oxidization of nitrogen oxides (NOx) into HONO through oxidants such as •OH and O_3, and HONO gas combines with inorganic cations in the atmosphere to form NO_3^- (Feng et al., 2018; Li et al., 2022). The study on the oxidation ratios of NO_2 to NO_3^-, SO_2 to SO_4^{2-}, and conversion ratio of NH_3 to NH_4^+ are critical, which could be calculated in

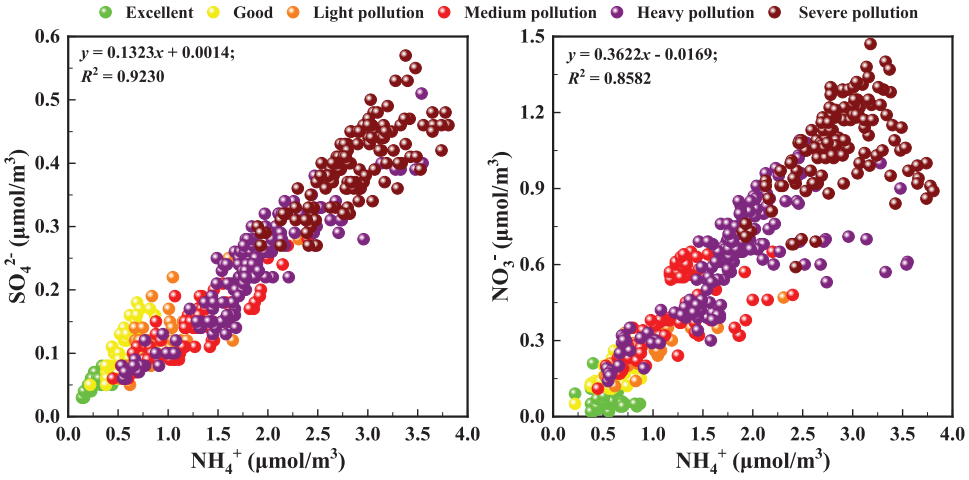

Fig. 4 – Scatter plots of ammonium verse sulfate (left) and ammonium verse nitrate (right).

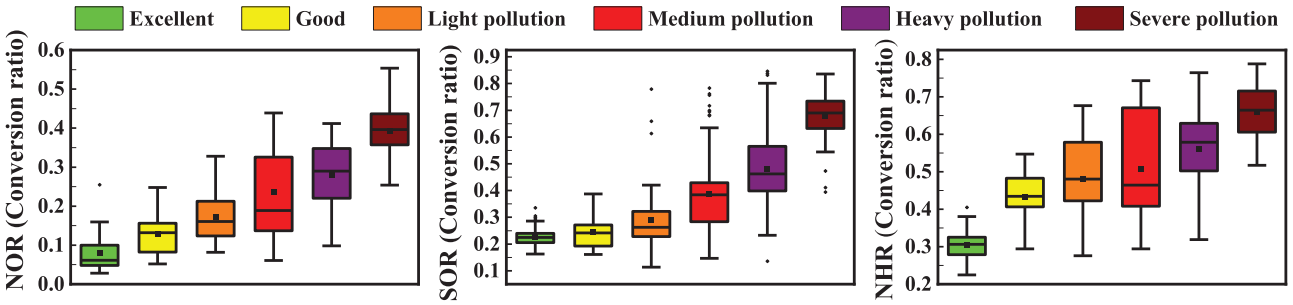

Fig. 5 – Box plots of the conversion ratios (SOR, NOR, and NHR) at different pollution levels.

the following equations.

$$NOR = [NO_3^-]/([NO_3^-] + [NO_2]) \quad (2)$$

$$SOR = [SO_4^{2-}]/([SO_4^{2-}] + [SO_2]) \quad (3)$$

$$NHR = [NH_4^+]/([NH_4^+] + [NH_3]) \quad (4)$$

where, NOR represents the nitrogen oxidation ratios, expressed as the molar concentration ratio of NO_3^- (μmol/m^3) to total NO_3^- and NO_2 (μmol/m^3). Similarly, SOR represents the sulfur oxidation ratios expressed as the molar concentration ratio of SO_4^{2-} (μmol/m^3) to the sum of SO_4^{2-} (μmol/m^3) and SO_2. Furthermore, NHR represents the ammonia conversion ratios, expressed as the molar ratio of NH_4^+ (μmol/m^3) to the sum of NH_4^+ and NH_3 (μmol/m^3).

Fig. 5 illustrates the oxidation ratios under different pollution levels. The average

NOR is 0.26 ± 0.12 with a maximum of 0.55, which shows at 15:00 on January 6th, 2019 (within the First haze episode). The average NOR shows an exponential upward trend (390%) with the increases of $PM_{2.5}$, from 0.08 ± 0.00 during the Excellent to 0.39 ± 0.06 during the Severe pollution. For SOR, the average value is 0.46 ± 0.19, while the maximum of 0.85 is seen at 14:00 on January 11th, 2019 (within the Second haze episode). SOR also shows an increasing trend (199%) with the $PM_{2.5}$ pollution, from 0.23 ± 0.04 to 0.68 ± 0.07 (from Excellent to Severe pollution). The average NHR is 0.54 ± 0.13, with a maximum of 0.79 at 00:00 on January 6th, 2019 (within the Second haze episode). Consistent with NOR and SOR, NHR also shows an increasing trend along the higher degrees of pollution, raised from 0.31 ± 0.04 to 0.66 ± 0.07 with an increasing rate of 116%. Generally, the NHR value is relatively low when the concentration of NH_3 in the atmosphere is high, and vice versa. If the NH_3 emissions are relatively stable and the degree of air pollution increases, more gaseous NH_3 would be converted into particulate NH_4^+ (Zhang et al., 2021). It should be noted that the conversion ratios (i.e., SOR, NOR, NHR) > 0.1 represent that the secondary conversion plays an important role in pollution (Bao et al., 2022). The larger the value, the stronger the secondary conversion.

During the observation period, 97% of hourly SOR, NOR, and NHR are greater than 0.1, demonstrating that secondary conversion is predominated in Xianyang. Especially, the average and maximum values of SOR are significantly higher than those of NOR. This reflects that the liquid-phase reaction of SO_2 is the main pathway to generate SO_4^{2-} during heavy pollution periods. From Excellent to Severe pollution levels, the secondary conversion ratios show robust growth trends, further supporting the significance of gas precursors participating in the secondary aerosol formation and deterioration of the air quality gradually.

In addition, meteorological parameters and NH_3 are important factors affecting the formation of secondary aerosols (Du et al., 2021), while the degree of the liquid phase reaction can be characterized by the magnitude of RH (Ervens et al., 2011). In addition, evaluating the formation of secondary aerosols with the conversion ratio can eliminate the influence of meteorological factors such as BLH.

Fig. 6a-c illustrates the variations of NOR, SOR, and NHR with RH. All are positively correlated ($P < 0.01$). Among them, the correlation between SOR and RH is the highest ($R^2 = 0.974$). The average value increases from 0.23 ± 0.04 (RH < 30%) to 0.72 ± 0.08 (90% ≤ RH < 100%), with an ascending rate of 213%. The correlation between NOR and RH is comparatively lower ($R^2 = 0.871$). When RH < 90%, NOR increases significantly with the increases of RH. When RH ≥ 90%, the RH increase, and the average value of NOR shows a slightly downward trend. The phenomenon has been discussed in the previous section. NHR and RH also have a significant correlation ($R^2 = 0.655$, $P < 0.01$). When RH < 80%, NHR increases with the RH, and reaches the maximum of 0.62 ± 0.07, indicating that with the increase of RH in a certain range, the increase of NH_3 participated in the particulate phase. At RH ≥ 80%, NHR shows a downward trend the same as NOR at RH ≥ 90%. The results of both the conversion ratios indicate the heterogeneous reaction is a key factor in the formation of SNA in Xianyang during the haze episode, consistent with the observation in Beijing, China (Zheng et al., 2015). Previous studies have shown that the aqueous oxidation of SO_2 by NO_2 can lead to the formation of large amounts of sulfate when the concentration of NH_3 and RH are high during heavy haze (Cheng et al., 2016). Particularly, SO_4^{2-} could increase the hygroscopicity of the particles, which might be the most critical step in the initial liquid phase chemistry (Wang et al., 2016a). Moreover, the high sulfur conversion ratio not only contributes to the formation of SO_4^{2-} but is also an important reason for promoting the formation of NO_3^- in the liquid phase (Wang et al., 2016a). The different trends

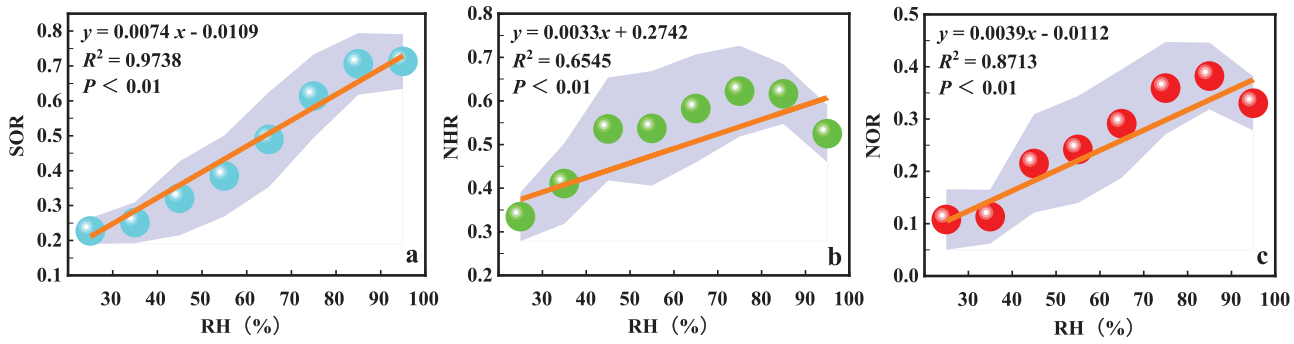

Fig. 6 – Variations of SOR, NHR, and NOR as a function of RH (a-c) during the observation period. The points and the light blue shadows indicate the mean values and error margins of SOR, NHR, and NOR in each bin (ΔRH = 10%).

of the conversion ratio could indicate that the higher RH was more conducive to the liquid-phase formation of SO_4^{2-} and elevate the conversion ratio of NH_3 through the gas-to-particulate phases significantly, promoting the formation and growth of WSIIs and $PM_{2.5}$. In specific, NH_3 could react with acidic substances that convert NH_3 to particulate NH_4^+, further leading to an increase of fine particles (Park et al., 2021; Saraswati et al., 2019; Swelum et al., 2021; Wang et al., 2015).

The SOR and NOR values are not only governed by the liquid-phase reaction but also affected by the molar concertation levels of ammonium. As shown in Fig. 7**a**, there is a significant correlation between SOR and NH_x ($R^2 = 0.9679$) (i.e., NH_x is the sum of the molar concentration of NH_3 and NH_4^+ (Fu et al., 2017)), indicating that the secondary formation of sulfate is closely related to the neutralization reaction of NH_x. Furthermore, SO_2 is more preferentially neutralized with ammonia and converted into secondary pollutants than NO_2 at high-RHs (Feng et al., 2018; Wang et al., 2016a). During the observation period, the humidity is relatively high, and fine particles are moderately acidic with a pH ranging from 3.0 to 4.9 in northern China (Liu et al., 2017; Zhang et al., 2021), possibly leading to ammonium reacting adequately with sulfate rather than nitrate. Therefore, the residual NH_x after the maximum neutralization with sulfate (i.e., Free-NH_3) is used to analyze its relationship with NOR.

As shown in Fig. 7**b**, a strong correlation between NOR and Free-NH_3 ($R^2 = 0.903$) is shown. The average NOR increased from 0.08 ± 0.03 (Free-NH_3 < 1.0) to 0.41 ± 0.02 (6.0 ≤ Free-NH_3 < 6.5), with an increasing rate of 413%. This supports the hypothesis that the higher degree of ammonia enrichment, the more conducive to the formation of NO_3^- in aerosol (Ge et al., 2019a).

Furthermore, even a higher SOR (0.57 ± 0.15) than NOR (0.33 ± 0.09) is observed during the heavy haze, the higher concentrations of gas precursors NO_2 (74.69 ± 16.54 μg/m^3) than SO_2 (13.83 ± 5.29 μg/m^3) led to more nitrate formation. In addition, the study area is in an ammonia-rich environment with high humidity, which promotes the heterogeneous reaction of nitrate. Therefore, nitrate is the highest inorganic ion during the campaign.

2.3. *Recognition of haze episodes*

As listed in Table 3, during the haze episodes, the strongest correlation with the $PM_{2.5}$ mass concentration is Free-NH_3 ($r = 0.76$), followed by RH ($r = 0.73$), WS ($r = 0.42$), and BLH ($r = 0.30$) at $P < 0.01$. Moreover, the $PM_{2.5}$ mass is also significantly correlated with NOR ($r = 0.79$), SOR ($r = 0.82$), NHR ($r = 0.68$), and SNA ($r = 0.92$) at $P < 0.01$, indicating that the transformation of SNA plays an important role in the growth of $PM_{2.5}$. Ox and $PM_{2.5}$ are significantly correlated at $P < 0.05$, while Ox has stronger significance with SNA at $P < 0.01$, demonstrating that oxidation capacity poses greater influences on the formation of SNA than $PM_{2.5}$. The $PM_{2.5}$ mass is negatively correlated with T and P at $P < 0.01$. The correlation analysis additionally proves that the growth of $PM_{2.5}$ is perceptibly related to higher Free-NH_3 and RH, which elevates the conversion ratio and facilitates the SNA formations.

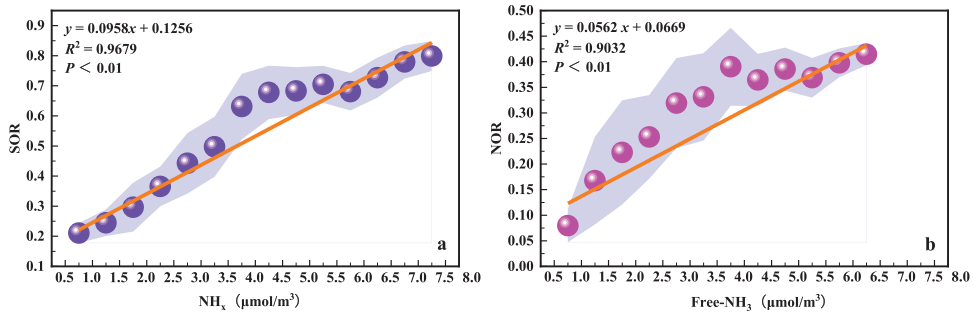

Fig. 7 – Variations of SOR as a function of NH_x (a), and NOR as a function of Free-NH_3 (b) during the observation period. The points and the light blue shadows indicate the mean values and error margins of SOR and NOR in each bin (both ΔNH$_x$ and ΔFree-NH_3 are 0.5 μmol/m^3).

Table 3 – Pearson correlation of $PM_{2.5}$, secondary conversion ratio, Ox, main meteorological elements, and Free-NH_3 during the observation period.

r	$PM_{2.5}$	T	WS	RH	P	BLH	Free-NH_3	O_x	NHR	NOR	SOR	SNA
$PM_{2.5}$	1.00											
T	-0.25**	1.00										
WS	-0.42**	0.23**	1.00									
RH	0.73**	-0.50**	-0.47**	1.00								
P	-0.16**	-0.37**	0.04	-0.19**	1.00							
BLH	-0.30**	0.45**	0.37**	-0.42**	0.05	1.00						
Free-NH_3	0.76**	-0.09	-.389**	.708**	-.282**	-.107*	1.00					
Ox	0.11*	0.67**	-0.02	-0.27**	-0.35**	0.14**	0.04	1.00				
NHR	0.68**	-0.17**	-0.15**	0.49**	-0.04	-0.17**	0.36**	0.20**	1.00			
NOR	0.79**	-0.12**	-0.19**	0.68**	-0.22**	-0.06	0.71**	0.02	0.81**	1.00		
SOR	0.82**	-0.21**	-0.33**	0.83**	-0.26**	-0.23**	0.84**	0.01	0.64**	0.85**	1.00	
SNA	0.92**	-0.12**	-0.30**	0.68**	-0.21**	-0.16**	0.80**	0.18**	0.78**	0.91**	0.90**	1.00

** Correlation is significant at the 0.01 level (two-tailed);
* Correlation is significant at the 0.05 level (two-tailed).
N = 498.

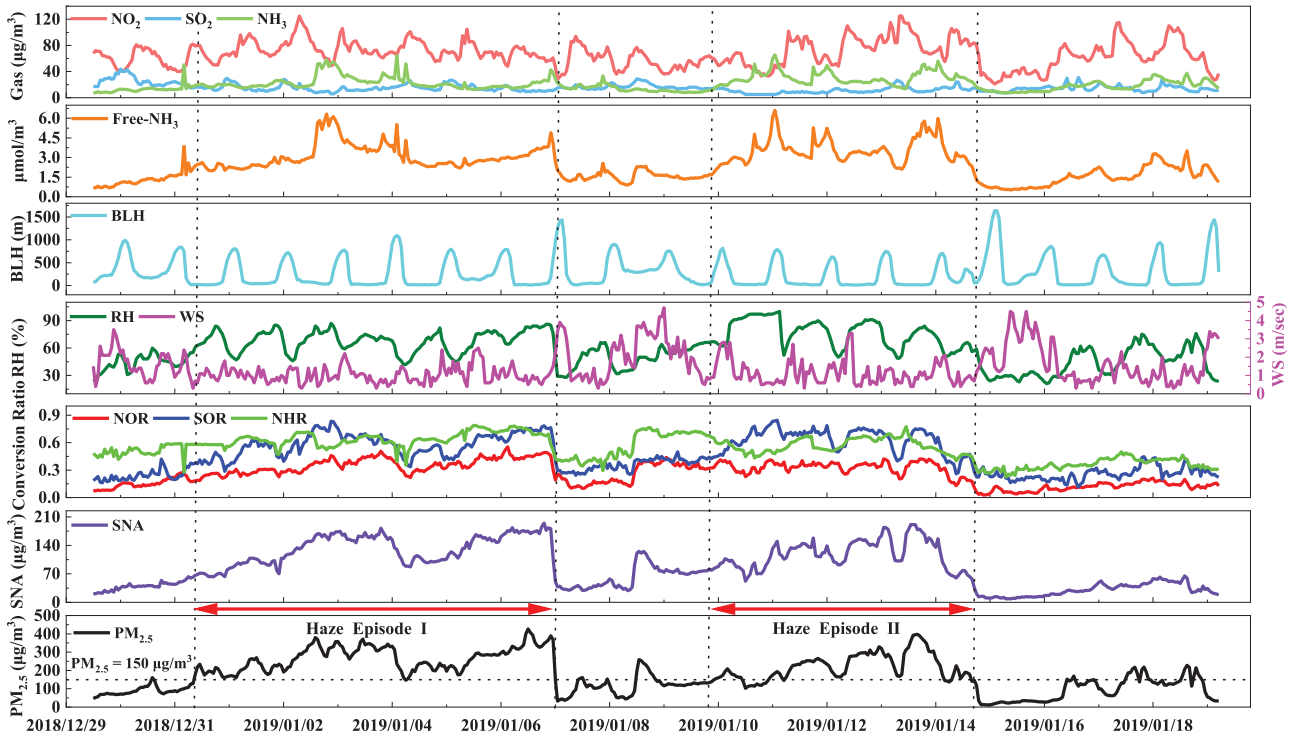

Fig. 8 – Temporal variations of concentrations of $PM_{2.5}$, gas precursors (NO_2, SO_2, and NH_3), Free-NH_3, and SNA, and the conversion ratios (NOR, SOR, and NHR), meteorological factors (wind speed, humidity, and boundary layer height) in a time interval of 1 hr during two haze episodes.

In addition, due to the low WS and BLH, air pollutants would be further accumulated.

As shown in Fig. 8, the concentrations of $PM_{2.5}$ and SO_2 at 00:00 on December 30th are relatively low but show a fluctuating upward trend, especially SO_2, which rapidly increases from 18 μg/m^3 at 00:00 to 44 μg/m^3 (the highest in the observation period) at noon on January 30th, 2018. The elevation of SO_2 is more obvious before the occurrence of the first haze episode. From 15:00 on December 30th to 21:00 on December 31st, 2018, the WS decreases from 1.9 to 0.7 m/s, reaching a stabilized atmospheric condition and leading to unfavorable air pollutants dispersion. Meanwhile, the RH increases from 31% to 61%, and the Free-NH_3 concentration increases from 0.70 to 1.14 μmol/m^3. During this period, the SO_2 concentrations then drop from 43 to 16 μg/m^3 rapidly, but NO_2 raise from 47 to 79 μg/m^3. The SNA concentration increases from 40.5 to 66.5 μg/m^3, as well as the $PM_{2.5}$ concentration rapidly rises from 75 to 178 μg/m^3, defined as a heavy pollution condition. This could be ascribed to SO_2 being preferentially neutralized with ammonia and more converted into secondary pollutants

than NO_2 at high-RH conditions (Feng et al., 2018; Wang et al., 2016a). Simultaneously, the conversion ratios show upward trends, of which NOR increase from 0.16 to 0.18, SOR from 0.19 to 0.38, and NHR from 0.49 to 0.58. The rapid increases in secondary conversion ratios indicate that SOR, NOR, and NHR are involved in multiphase and heterogeneous reactions in the process of haze formation, especially SOR (Acharja et al., 2022).

From 22:00 on December 31st, 2018 to 0:00 on January 7th, 2019, the average WS decreases from 1.6 ± 0.7 to 1.1 ± 0.5 m/sec, and maintain the same level during most of the hours, while the BLH decreases from 372.7 ± 280.0 to 240.9 ± 290.7 m. The two parameters demonstrate a relatively steady air movement status. RH presents an upward trend, showing an average value of 67.17% ± 11.07% and a maximum of 89%. Free-NH_3 also increases gradually, with an average of 3.08 ± 0.97 μmol/m^3 and a peak of 6.32 μmol/m^3.

The abovementioned chemical and methodological conditions lead to higher SOR, NOR, and NHR, with the average and maximum of 0.57 ± 0.12 (0.84), 0.35 ± 0.08 (0.55), 0.64 ± 0.08 (0.79), respectively. These would be further advanced by the greater accumulation of local pollutants under low WS and BLH (Hu and Wang, 2021; Wang et al., 2021). The higher RH and Free-NH_3 promote the rapid conversions of the gas precursors to particular ions, resulting in the SNA increase from 68.2 to 175.3 μg/m^3. During the First episode, the $PM_{2.5}$ concentration rose from 220 to 427 μg/m^3, and the degree of pollution reached the heaviest across the entire observation period. During the heavy haze in Xianyang, the meteorological characteristics include poor air diffusion capacity and high RH, which favor heterogeneous chemistry and lead to an increase in secondary aerosol formation. These reaction mechanisms are closely related to humidity to a large extent, which is consistent with the causes of haze in the city (Acharja et al., 2022; Elser et al., 2016; Li et al., 2017; Wang et al., 2014).

From 10:00 to 13:00 on January 7th, 2019, the methodological condition greatly varied, including WS increasing from 1.2 to 3.4 m/sec, BLH rising from 179.4 m to 1,251 m, RH dropping rapidly from 85% to 29%, and the Free-NH_3 decreasing from 4.90 to 1.82 μmol/m^3. Meanwhile, the conversion ratios also drop rapidly, and NOR, SOR, and NHR decline from 0.46 to 0.25, 0.76 to 0.29, and 0.58 to 0.41, respectively. The pollutants that accumulated for a long period would dissipate rapidly in both horizontal and vertical directions. The decline of RH also limits the conversion of secondary pollutants. These consequent atmospheric reactions lead to a sharp decline of $PM_{2.5}$ from 389 to 32 μg/m^3.

The second haze episode occurred under similar conditions as the first one, formulated by low WS, low BLH, high RH, and high ammonia-rich concentration. During the period from 11:00 on January 10th, 2019 to 04:00 on January 14th, 2019, the average WS is 1.2 ± 0.7 m/sec, while the BLH is 191.3 ± 261.9 m, even lower than that of the first haze episode by 50 m. The average RH is 76.0 ± 14.1% during this episode period, in which 84% of the time RH > 80%. It should be noted that the maximum RH even reaches ~100%. Moreover, the average and the maximum of Free-NH_3 are 3.48 ± 0.86 and 6.60 μmol/m^3, respectively. Meanwhile, high SOR, NOR, and NHR are also observed, with the average and the maximum of 0.65 ± 0.11 (0.85), 0.34 ± 0.05 (0.42), and 0.60 ± 0.06 (0.78), respectively. The secondary conversion ratios including SOR and NOR in Xianyang are slightly lower than those of Delhi, India (Kotnala et al., 2022), but significantly higher than those of Wuhan in Central China, Zibo and Beijing in North China, Harbin in Northeast China, and adjacent city Xi'an in Northwest China (Cheng et al., 2020; Li et al., 2022; Lu et al., 2021; Shen et al., 2021; Zhang et al., 2021), representing that the gas precursors in Xianyang city are more likely to be converted into secondary particulate matter than other cities of China. The SNA concentrations increased from 85.8 μg/m^3 at 11:00 on January 10th, 2019 to 191.0 μg/m^3 at 02:00 on January 14th, 2019, the highest in this episode event, while the $PM_{2.5}$ reached the highest of 397 μg/m^3 after 2 hr. The contributions of SNA to the haze episode are thus perceptible. This further indicates that the high RH during the heavy haze period promote the liquid-phase chemistry, which results in the increases of SO_4^{2-} and NO_3^-, and thus causes the continuously substantial increase of $PM_{2.5}$ (Cheng et al., 2016). From 07:00 on January 14th to 11:00 on January 15th, the WS increases from 1.2 to 2.4 m/s, and BTH increases from 18.0 to 861.2 m, advancing the horizontal and vertical dispersion of pollutants. Moreover, the RH shows a downward trend from 85% to 26%, while the concentration of Free-NH_3 decreases from 5.78 to 0.74 μmol/m^3 simultaneously. In addition, the conversion ratios drop rapidly which NOR from 0.41 to 0.03, SOR from 0.74 to 0.27, and NHR from 0.54 to 0.27. Conclusively, the gradual decrease of RH suppresses the generation of secondary pollutants. Meanwhile, SNA greatly decreases from 166.9 to 11.0 μg/m^3, and the $PM_{2.5}$ concentrations decline from 361 to 12 μg/m^3.

As for the interpretation of the causes of the haze episodes, both meteorological factors cannot be controlled, but the anthropogenic emission sources could be governed by controlling emissions in this area. The reductions of precursors especially NO_x and NH_3 could certainly suppress the formations of SNA, limit the growth of $PM_{2.5}$ and the formation of haze.

3. Conclusions

This study demonstrates the characteristics of WSII and their formation correlations with gas precursors and meteorological factors during the period of air quality deterioration from excellent to severe grades. From the perspective of the formation mechanism of SNA, the secondary conversion ratios for NOR, SOR, and NHR are greater than 0.1 from their corresponding precursor gases. Such conversion ratios also show upward trends along the air quality deteriorating from excellent to severe grades, indicating that strong secondary conversion is one of the critical factors of haze formation. RH also shows a great contribution to the secondary conversion ratios. It drives the liquid and heterogeneous reactions, promoting the SNA formations. In contrast, the higher degree of ammonia-rich, the more favorable condition for the distribution of HNO_3 into the particle phase and the formation of nitrate aerosols. The low WS and BLH cause the accumulation of air pollutants. Meanwhile, the high Free-NH_3 and RH further enhance the generation of SNA, and further deteriorate the air quality. Therefore, reductions in the emissions of the gas precursors, especially NO_x and NH_3, are essential to reduce the formation of SNA, as well as $PM_{2.5}$ pollution, in Xianyang.

Declaration of Competing Interest

The authors declare that they have no known competing financial interests or personal relationships that could have appeared to influence the work reported in this paper.

Acknowledgments

This work was supported by the National Key R&D Program of China (No. 2022YFF0802501), the Key Research and Development Program of Shaanxi Province (No. 2018-ZDXM3-01), and the Youth Innovation Promotion Association of the Chinese Academy of Sciences (No. 2019402).

Appendix A Supplementary data

Supplementary material associated with this article can be found in the online version at doi:10.1016/j.jes.2023.03.022.

References

Acharja, P., Ali, K., Ghude, S.D., Sinha, V., Sinha, B., Kulkarni, R., et al., 2022. Enhanced secondary aerosol formation driven by excess ammonia during fog episodes in Delhi, India. Chemosphere 289, 133155.

Alghamdi, M.A., Khoder, M., Harrison, R.M., Hyvärinen, A.P., Hussein, T., Al-Jeelani, H., et al., 2014. Temporal variations of O_3 and NOx in the urban background atmosphere of the coastal city Jeddah, Saudi Arabia. Atmos. Environ. 94, 205–214.

Allen, H.M., Draper, D.C., Ayres, B.R., Ault, A., Bondy, A., Takahama, S., et al., 2015. Influence of crustal dust and sea spray supermicron particle concentrations and acidity on inorganic NO_3^- aerosol during the 2013 Southern oxidant and aerosol study. Atmos. Chem. Phys. 15 (18), 10669–10685.

Bao, J.M., Li, H., Wu, Z.H., Zhang, X., Zhang, H., Li, Y.F., et al., 2022. Atmospheric carbonyls in a heavy Ozone pollution episode at a metropolis in Southwest China: characteristics, health risk assessment, sources analysis. J. Environ. Sci. 113, 40–54.

Bei, N.F., Li, X., Wang, Q.Y., Liu, S.X., Wu, J.R., Liang, J.Y., et al., 2021. Impacts of aerosol-radiation interactions on the wintertime particulate pollution under different synoptic patterns in the Guanzhong Basin, China. Adv. Atmos. Sci. 38 (7), 1141–1152.

Bei, N.F., Xiao, B., Meng, N., Feng, T., 2016. Critical role of meteorological conditions in a persistent haze episode in the Guanzhong basin, China. Sci. Total Environ. 550, 273–284.

Cao, J.J., Shen, Z.X., Chow, J.C., Watson, J.G., Lee, S.C., Tie, X.X., et al., 2012. Winter and summer $PM_{2.5}$ chemical compositions in fourteen Chinese cities. J. Air Waste Manage. Assoc. 62 (10), 1214–1226.

Chang, S.-Y., Lee, C.-T., Chou, C.C.K., Liu, S.-C., Wen, T.-X., 2007. The continuous field measurements of soluble aerosol compositions at the Taipei aerosol supersite, Taiwan. Atmos. Environ. 41 (9), 1936–1949.

Cheng, B.W., Ma, Y.X., Feng, F.L., Zhang, Y.F., Shen, J.H., Wang, H., et al., 2021. Influence of weather and air pollution on concentration change of $PM_{2.5}$ using a generalized additive model and gradient boosting machine. Atmos. Environ. 255.

Cheng, Y.F., Zheng, G.J., Wei, C., Mu, Q., Zheng, B., Wang, Z.B., et al., 2016. Reactive nitrogen chemistry in aerosol water as a source of sulfate during haze events in China. Sci. Adv. 2, e1601530.

Cheng, Y., Yu, Q.Q., Liu, J.M., Du, Z.Y., Liang, L.L., Geng, G.N., et al., 2020. Secondary inorganic aerosol during heating season in a megacity in Northeast China: evidence for heterogeneous chemistry in severe cold climate region. Chemosphere 261, 127769.

Clapp, L.J., Jenkin, M.E., 2001. Analysis of the relationship between ambient levels of O_3, NO_2 and NO as a function of NOx in the UK. Atmos. Environ. 35, 6391–6405.

Du, X., Yang, J., Xiao, Z., Tian, Y., Chen, K., Feng, Y., 2021. Source apportionment of $PM_{2.5}$ during different haze episodes by PMF and random forest method based on hourly measured atmospheric pollutant. Environ Sci Pollut. Res. Int. 28 (47), 66978–66989.

Elser, M., Huang, R.J., Wolf, R., Slowik, J.G., Wang, Q.Y., Canonaco, F., et al., 2016. New insights into $PM_{2.5}$ chemical composition and sources in two major cities in China during extreme haze events using aerosol mass spectrometry. Atmos. Chem. Phys. 16 (5), 3207–3225.

Ervens, B., Turpin, B.J., Weber, R.J., 2011. Secondary organic aerosol formation in cloud droplets and aqueous particles (Aqsoa): a review of laboratory, field and model studies. Atmos. Chem. Phys. 11 (21), 11069–11102.

Feng, T., Bei, N.F., Zhao, S.Y., Wu, J.R., Li, X., Zhang, T., et al., 2018. Wintertime nitrate formation during haze days in the Guanzhong Basin, China: a case study. Environ. Pollut. 243 (Pt B), 1057–1067.

Fu, X., Wang, S., Xing, J., Zhang, X.Y., Wang, T., Hao, J.M., 2017. Increasing ammonia concentrations reduce the effectiveness of particle pollution control achieved via SO_2 and NOx emissions reduction in East China. Environ. Sci. Technol. Lett. 4 (6), 221–227.

Ge, B.Z., Xu, X.B., Ma, Z.Q., Pan, X.L., Wang, Z., Lin, W.L., et al., 2019a. Role of ammonia on the feedback between AWC and inorganic aerosol formation during heavy pollution in the North China plain. Earth Space Sci. 6 (9), 1675–1693.

Ge, S.S., Wang, G.H., Zhang, S., Li, D.P., Xie, Y.N., Wu, C., et al., 2019b. Abundant NH_3 in China enhances atmospheric hono production by promoting the heterogeneous reaction of SO_2 with NO_2. Environ. Sci. Technol. 53 (24), 14339–14347.

Han, Y., Wang, Z.C., Zhou, J.W., Che, H.X., Tian, M., Wang, H.B., et al., 2021. $PM_{2.5}$-bound heavy metals in Southwestern China: characterization, sources, and health risks. Atmosphere 12 (7).

Huang, R.J., Duan, J., Li, Y.J., Chen, Q., Chen, Y., Tang, M.J., et al., 2020. Effects of NH_3 and alkaline metals on the formation of particulate sulfate and nitrate in wintertime Beijing. Sci. Total Environ. 717, 137190.

Huang, X.J., Zhang, J.K., Zhang, W., Tang, G.Q., Wang, Y.S., 2021. Atmospheric ammonia and its effect on $PM_{2.5}$ pollution in urban Chengdu, Sichuan Basin, China. Environ. Pollut. 291, 118195.

Hu, Y.L., Wang, S.G., 2021. Formation mechanism of a severe air pollution event: a case study in the Sichuan Basin, Southwest China. Atmos. Environ. 246.

Jain, C.D., Ratnam, M.V., Madhavan, B.L., Sindhu, S., Kumar, A.H., 2022. Impact of regional transport on total O_X (NO_2+ O_3) concentrations observed at a tropical rural location. Atmos. Pollut. Res. 13 (5).

Jenkin, M.E., 2014. Investigation of an oxidant-based methodology for AOT40 exposure assessment in the UK. Atmos. Environ. 94, 332–340.

Kotnala, G., Sharma, S.K., Mandal, T.K., 2022. Long-term (2013-2018) relationship of water-soluble inorganic ionic species of $PM_{2.5}$ with ammonia and other trace gases in Delhi, India. Aerosol Sci. Eng. 6 (4), 349–359.

Kuang, Y., Xu, W.Y., Lin, W.L., Meng, Z.Y., Zhao, H.R., Ren, S.X., et al., 2020. Explosive morning growth phenomena of NH_3 on the North China Plain: causes and potential impacts on aerosol formation. Environ. Pollut. 257, 113621.

Li, G.H., Bei, N.F., Cao, J.J., Huang, R.J, Wu, J.R., Feng, T., et al., 2017. A possible pathway for rapid growth of sulfate during haze days in China. Atmos. Chem. Phys. 17 (5), 3301–3316.

Li, L., Wang, Q.Y., Zhang, Y., Liu, S.X., Zhang, T., Wang, S., et al., 2022. Impact of reduced anthropogenic emissions on chemical characteristics of urban aerosol by individual particle analysis. Chemosphere 303 (Pt 2), 135013.

Liu, F., Tan, Q.W., Jiang, X., Yang, F.M., Jiang, W.J., 2019a. Effects of relative humidity and $PM_{2.5}$ chemical compositions on visibility impairment in Chengdu, China. J. Environ. Sci. 86, 15–23.

Liu, M.X., Huang, X., Song, Y., Tang, J., Cao, J.J., Zhang, X.Y., et al., 2019b. Ammonia emission control in China would mitigate haze pollution and nitrogen deposition, but worsen acid rain. Proc. Natl. Acad. Sci. U.S.A. 116 (16), 7760–7765.

Liu, M.X., Song, Y., Zhou, T., Xu, Z.Y., Yan, C.Q., Zheng, M., et al., 2017. Fine particle PH during severe haze episodes in Northern China. Geophys. Res. Lett. 44 (10), 5213–5221.

Lobert, J.M., Keene, W.C., Logan, J.A., Yevich, R., 1999. Global Chlorine emissions from biomass burning: reactive chlorine emissions inventory. J. Geophys. Res. Atmos. 104 (D7), 8373–8389.

Lu, M.M., Tang, X., Feng, Y.C., Wang, Z.F., Chen, X.S., Kong, L., et al., 2021. Nonlinear response of SIA to emission changes and chemical processes over eastern and central China during a heavy haze month. Sci. Total Environ. 788, 147747.

Pancholi, P., Kumar, A., Bikundia, D.S., Chourasiya, S., 2018. An observation of seasonal and diurnal behavior of O_3-NO_x relationships and local/regional oxidant ($O_X = O_3 + NO_2$) levels at a semi-arid urban site of western India. Sustain. Environ. Res. 28 (2), 79–89.

Pang, N.N., Gao, J., Zhao, P.S., Wang, Y.L., Xu, Z.J., Chai, F.H., 2021. The impact of fireworks control on air quality in four Northern Chinese cities during the Spring Festival. Atmos. Environ. 244, 117958.

Park, J., Kim, E., Oh, S., Kim, H., Kim, S., Kim, Y.P., et al., 2021. Contributions of ammonia to high concentrations of $PM_{2.5}$ in an urban area. Atmosphere 12 (12).

Saraswati, Sharma, S.K., Saxena, M., Mandal, T.K., 2019. Characteristics of gaseous and particulate ammonia and their role in the formation of secondary inorganic particulate matter at Delhi. India. Atmos. Res. 218, 34–49.

Shen, L.J., Wang, H.L., Cheng, M.T., Ji, D.S., Liu, Z.R., Wang, L.L., et al., 2021. Chemical composition, water content and size distribution of aerosols during different development stages of regional haze episodes over the North China Plain. Atmos. Environ. 245.

Shen, Z.X., Arimoto, R., Cao, J.J., Zhang, R.J., Li, X.X., Du, N., et al., 2008. Seasonal variations and evidence for the effectiveness of pollution controls on water-soluble inorganic species in total suspended particulates and fine particulate matter from Xi'an, China. J. Air Waste Manage. Assoc. 58 (12), 1560–1570.

Sinha, J., Kumar, N., 2019. Mortality and air pollution effects of air quality interventions in Delhi and Beijing. Front. Environ. Sci. 7.

Swelum, A.A., El-Saadony, M.T., Abd El-Hack, M.E., Abo Ghanima, M.M., Shukry, M., Alhotan, R.A., et al., 2021. Ammonia emissions in poultry houses and microbial nitrification as a promising reduction strategy. Sci. Total Environ. 781.

Tian, J., Wang, Q.Y., Zhang, Y., Yan, M.Y., Liu, H.K., Zhang, N.N., et al., 2021. Impacts of primary emissions and secondary aerosol formation on air pollution in an urban area of China during the COVID-19 lockdown. Environ. Int. 150, 106426.

Tian, M., Wang, H.B., Chen, Y., Zhang, L.M., Shi, G.M., Liu, Y., et al., 2017. Highly time-resolved characterization of water-soluble inorganic ions in $PM_{2.5}$ in a humid and acidic Mega City in Sichuan Basin, China. Sci. Total Environ. 580, 224–234.

Wang, G.H., Zhang, R.Y., Gomez, M.E., Yang, L.X., Levy Zamora, M., Hu, M., et al., 2016a. Persistent sulfate formation from London Fog to Chinese Haze. Proc. Natl. Acad. Sci. U.S.A. 113 (48), 13630–13635.

Wang, J., Zhang, Y.-f., Feng, Y.-c., Zheng, X.-j., Jiao, L., Hong, S.-m., et al., 2016b. Characterization and source apportionment of aerosol light extinction with a Coupled Model of Cmb-Improve in Hangzhou, Yangtze River Delta of China. Atmos. Res. 178-179, 570–579.

Wang, Q.Y., Cao, J.J., Tao, J., Li, N., Su, X.L., Chen, L.W., et al., 2013. Long-term trends in visibility and at Chengdu, China. PLoS One 8 (7), 68894.

Wang, S.S., Nan, J.L., Shi, C.Z., Fu, Q.Y., Gao, S., Wang, D.F., et al., 2015. Atmospheric ammonia and its impacts on regional air quality over the Megacity of Shanghai, China. Sci. Rep. 5 (1).

Wang, Y., Shi, M.S., Lv, Z., Liu, H., He, K., 2021. Local and regional contributions to $PM_{2.5}$ in the Beijing 2022 Winter Olympics infrastructure areas during haze episodes. Front. Environ. Sci. 15 (6).

Wang, Y.X., Zhang, Q.Q., Jiang, J.K., Zhou, W., Wang, B.Y., He, K.B., et al., 2014. Enhanced sulfate formation during China's severe winter haze episode in January 2013 missing from current models. J. Geophys. Res. Atmos. 119 (17) 10,425-410,440.

Wen, Z., Wang, C.J., Li, Q., Xu, W., Lu, L., Li, X.J., et al., 2021. Winter air quality improvement in Beijing by clean air actions from 2014 to 2018. Atmos. Res. 259.

Wu, C., Wang, G.H., Li, J., Li, J.J., Cao, C., Ge, S.S., et al., 2020. Non-agricultural sources dominate the atmospheric NH_3 in Xi'an, a Megacity in the Semi-Arid Region of China. Sci. Total Environ. 722, 137756.

Xia, D.H., Jiang, B.F., Xie, Y.L., 2016. Modeling and analysis of $PM_{2.5}$ generation for key factors identification in China. Atmos. Environ. 134, 208–216.

Xu, H.M., Léon, J.-F., Liousse, C., Guinot, B., Yoboué, V., Akpo, A.B., et al., 2019. Personal exposure to $PM_{2.5}$ emitted from typical anthropogenic sources in Southern West Africa: Chemical characteristics and associated health risks. Atmos. Chem. Phys. 19 (10), 6637–6657.

Young, L.-H., Li, C.-H., Lin, M.-Y., Hwang, B.-F., Hsu, H.-T., Chen, Y.-C., et al., 2016. Field performance of a semi-continuous monitor for ambient $PM_{2.5}$ water-soluble inorganic ions and gases at a Suburban Site. Atmos. Environ. 144, 376–388.

Zhan, Y.Z.H., Xie, M., Gao, D., Wang, T.J., Zhang, M., An, F.X., 2021. Characterization and source analysis of water-soluble inorganic ionic species in $PM_{2.5}$ during a Wintertime particle pollution episode in Nanjing, China. Atmos. Res. 262.

Zhang, T., Shen, Z.X., Su, H., Liu, S.X., Zhou, J.M., Zhao, Z.Z., et al., 2021. Effects of aerosol water content on the formation of secondary inorganic aerosol during a winter heavy $PM_{2.5}$ pollution episode in Xi'an, China. Atmos. Environ. 252.

Zhang, X.M., Wu, Y.Y., Liu, X.J., Reis, S., Jin, J.X., Dragosits, U., et al., 2017. Ammonia emissions may be substantially underestimated in China. Environ. Sci. Technol. 51 (21), 12089–12096.

Zhao, Z.J., Liu, R., Zhang, Z.Y., 2020. Characteristics of winter haze pollution in the Fenwei Plain and the possible influence of EU during 1984-2017. Earth Space Sci. 7 (6).

Zheng, G.J., Duan, F.K., Su, H., Ma, Y.L., Cheng, Y., Zheng, B., et al., 2015. Exploring the severe winter haze in Beijing: the impact of synoptic weather, regional transport and heterogeneous reactions. Atmos. Chem. Phys. 15 (6), 2969–2983.